# Vortex pinning and critical currents in nanostructured novel superconductors

**Kušević, Ivica; Babić, Emil**

*Source / Izvornik:* **Fizika A, 2005, 14, 75 - 88**

**Journal article, Published version**
**Rad u časopisu, Objavljena verzija rada (izdavačev PDF)**

*Permanent link / Trajna poveznica:* https://urn.nsk.hr/urn:nbn:hr:217:030615

ISSN 1330–0008
CODEN FIZAE4

# VORTEX PINNING AND CRITICAL CURRENTS IN NANOSTRUCTURED NOVEL SUPERCONDUCTORS

IVICA KUŠEVIĆ and EMIL BABIĆ

*Department of Physics, Faculty of Science, University of Zagreb, HR-10000 Zagreb, Croatia*

**Dedicated to the memory of Professor Vladimir Šips**

Received 28 September 2004; Accepted 13 June 2005
Online 7 November 2005

A systematic analysis of the parameters associated with vortex pinning in novel superconductors containing nano-scale strong isotropic pinning centres (such as U/n processed Bi2223/Ag tapes and nanoparticle added $MgB_2$) has been carried out. Although the systems studied are very different as regards their structures, types of nano-scale defects and vortices, their pinning parameters (irreversibility fields and the fields for the maximum volume pinning force) show distinct common features. In particular, for moderate defect densities $n_\phi$, in all these systems the enhancement of the pinning parameters in nanostructured state is approximately linear in $n_\phi$ over sizable field and temperature windows. Accordingly, these systems exhibit a kind of matching effects with the effective matching field $B_\phi$, correlated with the areal density of defects. The field $B_\phi$ forms a natural field scale for the vortex pinning phenomena in such systems. However, at fields far from $B_\phi$, an interplay of different pinning mechanisms sets in. The impact of these results for the future enhancement of the flux pinning and critical currents in nanostructured Bi2223 and $MgB_2$ superconductors is briefly discussed.

PACS numbers: 74.60.Ge,74.60.Jg,74.62.Dh UDC 538.945
Keywords: novel superconductors, vortex pinning, U/n processed Bi2223/Ag, $MgB_2$

## 1. Introduction

The technological success of superconductors depends on our ability to produce wires capable of conducting large critical current densities $J_c$ in high magnetic fields. This task became feasible upon the discovery of type II superconductors which remain superconducting in fields $H \leq H_{c2}$ (upper critical field) well in ex-

cess of their thermodynamic critical field $H_c$. However, the quantized flux $\Phi_0$ and the associated vortex in these materials can move due to the Lorentz force imposed by current flow, which results in energy dissipation [1]. Flux motion can be prevented if the material contains imperfections that strongly and abruptly alter its superconducting properties over spatially small regions. This vortex pinning occurs because the condensation energy (lost in the normal vortex core) can be regained by positioning the vortex on a normal defect. The most effective defect size is set by the size of the vortex core $\sim \xi$ (the superconducting coherence length), and the optimal defect density $n$ is set by the field $B$ required in a given application.

The optimization of the conventional superconductors (LTS) relies mainly [2, 3] on the grain size (for compounds such as $Nb_3Sn$) and on simultaneous formation of the fine non-superconducting precipitates (for alloys such as NbTi). The unique combination of the vortex pinning by the grain boundaries and fine $\alpha$-Ti precipitates makes NbTi the most successful LTS.

The discovery [4] of high-temperature superconductors (HTS) made it possible to develop superconductors operating at both fields and temperatures well in excess of those attainable with LTS. However, high-angle grain boundaries (that form in untextured polycrystalline materials) in HTS form weak-links which limit $J_c$ and render untextured HTS useless for applications [5]. Further, large intrinsic anisotropy and short $\xi$ of HTS cause low-lying irreversibility fields ($J_c$ vanishes above $B_{irr}$) $B_{irr} \ll B_{c2}$ at elevated temperatures [6]. The problem of weak-links has been partially circumvented by using various grain alignment techniques (which reduce the areas of high-angle grain boundaries). In particular, large lengths of Bi2212/Ag and Bi2223/Ag composite tapes with $J_c$(4.2 K, 25 T) $\sim 10^5$ A/cm$^2$ have been made [7]. However, no commercial solution for the problem of weak flux pinning at elevated temperatures (low $B_{irr}$) has been found as yet [8]. At present, columnar defects (CD) with diameters ($c_0$) comparable to the superconducting coherence length ($\xi_{ab}$) are the most efficient flux pinning centers in HTS [8]. CDs can be produced either by irradiation of HTS with heavy ions or with fission of suitable atoms incorporated within HTS. The first method produces parallel CDs and yields uniaxial enhancement of flux pinning, whereas the other technique produces randomly splayed CDs with isotropic pinning [8]. In particular, irradiation of $^{235}$U-doped Bi2223/Ag tapes with thermal neutrons ("U/n" treatment) causes, both for field $B$ parallel to the $c$-axis of Bi2223 grains and perpendicular to it, large enhancements of the irreversibility field $B_{irr}$ and field $B_{max}$ (the pinning force density $F_p = J_c B$ reaches its maximum at $B = B_{max}$) [9].

The discovery of superconductivity in $MgB_2$ compound [10] with $T_c \simeq 39$ K made $MgB_2$ a promising material [11] for the applications at $T \geq 20$ K, which is above $T_c$s of LTS. Indeed, simple preparation, the absence of weak links [12, 13, 14] and rather high $J_c$ of composite $MgB_2$ wires [13, 15, 16, 17, 18] lend strong support to these expectations. Unfortunately, compared to practical LTS (NbTi, $Nb_3$ Sn), $MgB_2$ exhibits weak flux-pinning [11, 19], which results in low irreversibility field $B_{irr}$(4.2 K) $\approx 8$ T [11]. Several techniques, such as alloying [20, 21, 22], particle irradiation [23, 24, 25] and mechanical processing [18, 26] have been employed in order to improve the flux-pinning in $MgB_2$, but with limited success. Better results

were recently obtained by adding nanoparticles to $MgB_2$ [27, 28, 29] . It appears that a variety of nanoparticles considerably enhance the flux-pinning in $MgB_2$ over a wide temperature range $T \leq 30$ K. In particular, the addition of 10 wt% of SiC nanoparticles [28] yielded $B_{\rm irr}(4.2\ {\rm K}) \gtrsim 12$ T, which is higher than that of optimized NbTi [2]. Nanoparticles usually form nanoprecipitates [28] with size $\sim \xi$ [11] within the $MgB_2$ matrix, which ensure an efficient vortex pinning [30].

Here we compare the results for high-temperature magnetoresistance $R(T, B)$ and critical current density $J_{\rm c}(T, B)$ of $MgB_2$ tapes doped with Si-nanoparticles with those for U/n treated Bi2223/Ag tapes. Our results show strong similarity in the variation of the vortex pinning parameters ($B_{\rm irr}(T)$, $B_{\rm max}(T)$) of these two nanostructured systems. In particular, in both systems vortex pinning depends on the density of nano-scale defects and both systems show the strongest enhancement of the pinning parameters when the defect density approximately matches that of the vortices. The impact of these results for the future development in bulk nanostructured superconductors is briefly discussed.

## 2. *Experimental procedures*

The Ag-sheathed $Bi_{1.83}Pb_{0.35}Sr_{1.95}Ca_{2.05}Cu_{3.05}O_x$ (hereafter Bi2223) tapes were fabricated using the in-situ powder-in-tube technique [31]. Besides the control (undoped–unirradiated) sample, four samples with $^{235}$U-oxide ($UO_2 \cdot 2H_2O$) contents $c = 0.15$, 0.6 and 2 wt% (1wt% $^{235}$ U-oxide corresponds approximately to 0.33 at% $^{235}$U) were irradiated with different thermal neutron fluences $0.2 \cdot 10^{19} \leq \phi \leq 5 \cdot 10^{19}$ n/m$^2$. Fission of $^{235}$U atoms produced randomly splayed CDs with diameter $c_0 \approx 5$ nm and average length of 3 $\mu$m. Different $c$ and $\phi$ combinations resulted in four different fission track densities roughly proportional to $c\phi$, and from these parameters one can calculate [32] areal density of defects and the corresponding matching field $B_\phi$ (at which the areal density of CDs is approximately equal to the areal density of vortices).

Cu-sheathed $MgB_2$ tapes and wires were prepared by the in-situ powder-in-tube method [17]. In the doped samples, in addition to Mg (99%) and B (99%), $c \leq 10$ wt% of Si-nanoparticles with an average size $\sim 50$ nm was added. The total number of samples was five (tapes with $c = 0$, 5 and 10 wt% of Si and wires with $c = 0$ and 5 wt% of Si). A low sintering temperature (670 – 690°C) and short sintering times (six minutes in a high purity Ar gas) were employed [29] in order to avoid larger diffusion of Cu into the $MgB_2$ core [33]. This resulted in rather porous, low density ($\sim 50\%$) cores.

For both types of superconductors, samples were cut to an approximate length of 2 cm. Current and voltage contacts were soldered on the corresponding sheaths which were thinned with suitable etchants in order to increase the resistivity of sheath and, therefore, to increase the sensitivity of electrical measurements. Magnetoresistance measurements were performed with exciting ac (frequency 18.4 Hz) and $I_{\rm RMS} = 1$ mA, corresponding to a current density of $J \leq 1.4$ A/cm$^2$, variations in $J$ being the consequence of different cross-sectional areas. For some samples

of both types, we also used $I_{\mathrm{RMS}} = 10$ mA in order to verify that the observed $B_{\mathrm{irr}}(T)$ variation does not depend on the magnitude of current within the low-current regime. Magnetic field $B \leq 0.95$ T was applied perpendicular to the broad surface of tapes and perpendicular to the current direction in the temperature range 50 – 120 K (Bi2223) and 28 – 40 K ($MgB_2$). Critical currents $I_c(T, B)$ were measured with the pulse method (saw-tooth pulse with the duration 5 – 10 ms, maximum amplitude 200 A) with the electric field criterion 1 $\mu$V/cm. Some data relevant to our samples are given in Table 1.

*TABLE 1. Some data relevant to our samples: type of sample, c is the weight percentage of* Si ($MgB_2$ *samples*) *or* $UO_2{\cdot}2H_2O$ (Bi2223/Ag *samples*), $\phi$ *is the thermal neutron fluence,* $T_{c0}$ *is temperature of the resistivity onset,* $J_{c0}$ *is critical current density in zero field at* $T_s = 35$ K ($MgB_2$ *samples*) *and 77* K (Bi2223/Ag *samples*) *and* $B_\phi$ *is the matching field.*

| Sample | $c$ (wt%) | $\phi$ ($10^{19}$ n/m$^2$) | $T_{c0}$ (K) | $J_{c0}(T_s)$ (A/cm$^2$) | $B_\phi$ (T) |
|---|---|---|---|---|---|
| $MgB_2$ wire | 0 | | 38.1 | 3200 | |
| | 5 | | 36.6 | 8400 | 0.15 |
| $MgB_2$ tape | 0 | | 37.9 | 22800 | |
| | 5 | | 36.4 | 6600 | 0.3 |
| | 10 | | 36.5 | 2300 | 0.6 |
| Bi2223/Ag | 0 | 0 | 107.1 | 17000 | |
| tape | 2 | 0.2 | 104.6 | 12060 | 0.21 |
| | 0.15 | 5 | 107.0 | 17100 | 0.37 |
| | 0.6 | 1.25 | 107.4 | 20100 | 0.39 |
| | 0.6 | 1.75 | 107.2 | 18860 | 0.54 |

## 3. *Results and discussion*

In Fig. 1a and b we compare the effects of defects with size $\sim \xi$ (nanoprecipitates or CDs) on the high-temperature superconducting transitions of typical $MgB_2$/Cu and Bi2223/Ag tapes.

Fig. 1a compares the superconducting transitions in fields $B \leq 0.9$ T perpendicular to the tape plane for typical undoped and nanoparticle doped $MgB_2$ tape. As in other composite superconductors [34], the shape of these transitions is affected by Cu-sheathing. However, the onset of resistance (hence $T_c(R \to 0) = T_{c0}$) is not affected by sheathing [34]. Since two samples had different $R$(39 K) and $T_{c0}$ (Table 1) values, we show results in normalized scales, i.e. $R(T, B)/R(39\ \mathrm{K}, 0)$ vs. $t = T/T_{c0}(B = 0)$. A strong shift of $T_{c0}$ with magnetic field (i.e. $T_{\mathrm{irr}}(B)$) reflects a rather weak flux-pinning in the undoped $MgB_2$. For the doped sample, the shift of its $T_{c0}$ with field is sizably smaller, which indicates considerable enhancement

of flux-pinning (i.e. the expansion of the vortex-solid regime). Furthermore, values

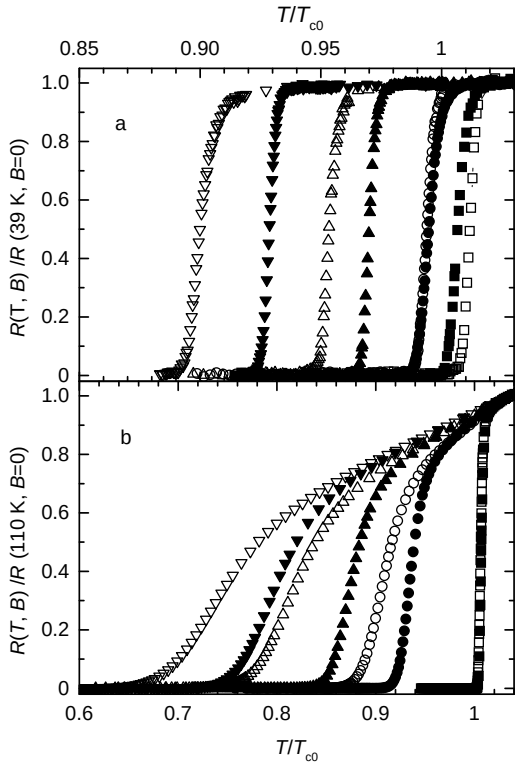


*Fig. 1. Temperature variation of the normalized electrical resistance for: a)* $MgB_2$ *undoped tape (empty symbols) and tape doped with 5 wt%* Si *(full) in magnetic fields* $B = 0(\square)$, *0.1* $(\bigcirc)$, *0.4* $(\triangle)$ *and 0.9 T* $(\nabla)$, *b) control* Bi2223/Ag *tape (empty) and* Bi2223/Ag *tape with* $B_\phi = 0.54$ *T (Table 1, full symbols) in* $B = 0(\square)$, *0.1* $(\bigcirc)$, *0.4* $(\triangle)$ *and 0.95 T* $(\nabla)$.

of $T_{c0}$ for the doped sample in $B \lesssim 0.3$ T are compressed within a rather narrow temperature interval, whereas those for the undoped one are more evenly spread throughout the explored field range. Qualitatively the same behaviour was observed for all nano-Si doped samples.

Fig. 1b compares the superconducting transitions in fields $B \leq 0.95$ T perpendicular to the tape plane for control and U/n processed Bi2223 tape. The effect of U/n processing of Bi2223/Ag is qualitatively the same as that of nanoparticles in $MgB_2$ (Fig. 1a). However, the field-induced broadening of the superconducting transitions and the overall shift of $T_{c0}$ with $B$ is much larger for Bi2223/Ag tapes than that for the $MgB_2$ ones (Fig. 1a) which shows that at elevated temperatures ($t > 0.6$), vortex pinning in $MgB_2$ is much stronger than that in Bi2223 [14]. Qualitatively the same results were obtained for all U/n processed samples. Taken together, Figs. 1a and 1b show the enhancement of the irreversibility fields (resistive onsets) of the nanostructured samples relative to virgin ones for both systems over most of the explored $t$-range (i.e. except for $t \simeq 1$ [30, 35]).

In Figs. 2a and 2b, we show the temperature variations of $B_{irr}$ for all samples of both systems. Here we defined $B_{irr}$ with low-resistivity criterion (1 nΩcm and 5nΩcm for Bi2223/Ag and $MgB_2$/Cu samples, respectively) and use the tempera-

ture scales which fit the best $B_{\rm irr}(T)$ variations for the corresponding virgin samples [30, 35].

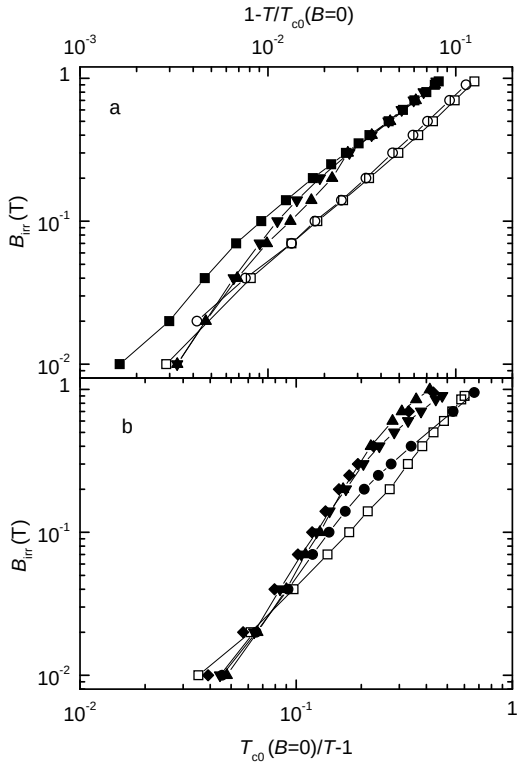


*Fig. 2. Temperature dependence of the irreversibility field $B_{\rm irr}$ in appropriate temperature scales for a)* $MgB_2$ *samples: undoped (□) and* Si*-doped (■) wire and undoped (○), 5 wt% (▲) and 10 wt%* Si*-doped tape (▼), and b)* Bi2223/Ag *tapes: undoped (□), $B_\phi = 0.21$ (●), 0.37 (▲), 0.39 (▼) and 0.54 T (♦).*

For our undoped $MgB_2$ samples (Fig. 2a), both the magnitudes and temperature variation of $B_{\rm irr}$ are practically the same as the literature data for bulk $MgB_2$ samples [11, 14, 25, 33, 36]. In particular, our values of $B_{\rm irr}(T)$ are equal to those obtained from the onset of the third harmonic in the low-frequency ac susceptibility of a dense $MgB_2$ sample [36], which shows that different methods for the determination of $B_{\rm irr}$ are equivalent (providing that criterion $J_{\rm c} \to 0$ is respected). Approximately linear, $B_{\rm irr}(t)$ variations for undoped samples below $t = 0.95$ extrapolate to $B_{\rm irr}(4.2\ {\rm K}) \approx 8$ T (wire) and 8.4 T (tape), which are typical values for bulk $MgB_2$ [11]. For the doped samples, $B_{\rm irr}$ increases initially rapidly with decreasing temperature and shows slower, approximately linear variation at low temperatures. The low-temperature $B_{\rm irr}(T)$ variations for doped samples extrapolate to $B_{\rm irr}(4.2\ {\rm K}) \approx 11$ T (5 wt% Si) and 11.5 T (10 wt% Si). These values are consistent with the other results for nanoparticle doped $MgB_2$ [27, 28, 29] and are higher than $B_{\rm irr}(4.2\ {\rm K})$ for optimized NbTi wires. Fig. 2a shows that for $t \leq 0.98$, $B_{\rm irr}$s of the doped samples are higher than those of the undoped samples. Therefore, vortex pinning in nanoparticle doped $MgB_2$ is enhanced relative to that in undoped $MgB_2$ at reduced temperatures $t_{\rm irr} \leq 0.98$. The plot of the ratio $B_{\rm irr}({\rm doped})/B_{\rm irr}({\rm undoped})$ vs. $t$ in Fig. 3a confirms this fact.

In spite of the vast difference in the superconducting properties between $MgB_2$ and Bi2223 systems, and equally large difference in the nature and topology of the

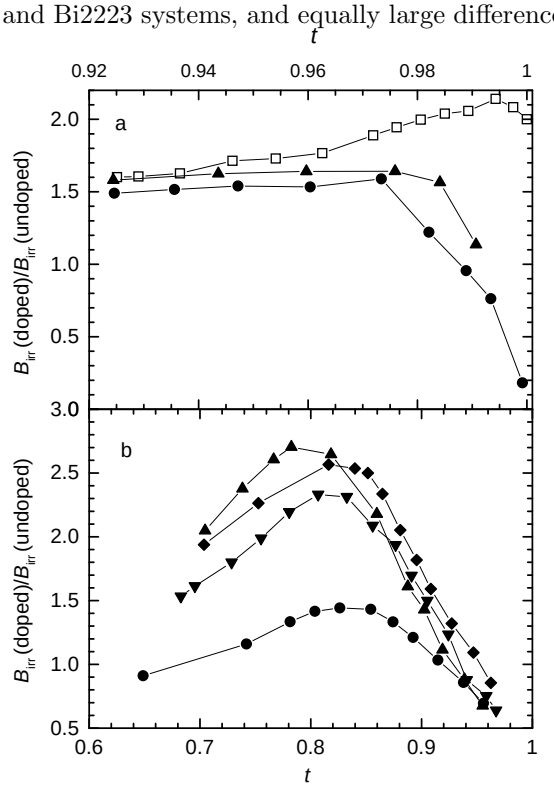


*Fig. 3. The ratio* $B_{\rm irr}(doped)/B_{\rm irr}(undoped)$ *vs. reduced temperature* $t = T/T_{\rm c0}$ *for a)* $MgB_2$ *5 wt% Si-doped wire (□) and tapes with* $c = 5$ *wt%* Si *(●) and 10 wt% (▲), and b)* Bi2223/Ag *tapes with* $B_\phi = 0.21$ *(●), 0.37 (▲), 0.39 (▼) and 0.54 T (♦).*

defects introduced in two systems, the behaviour of their $B_{\rm irr}(T)$ is qualitatively the same (Figs. 2a and 2b). In particular, $B_{\rm irr}(T)$ for U/n processed samples (Fig. 2b) is enhanced relative to that of the virgin sample over most of the temperature range ($t \leq 0.95$) and it also shows a change of slope on decreasing the temperature.

The change in the slope of $B_{\rm irr}(T)$ variation is specific for HTS containing columnar defects [6, 37, 38, 39], where the crossover in $B_{\rm irr}(T)$ occurs around the matching field $B_\phi = n_\phi \Phi_0$ [38, 39]. In HTS containing columnar defects (CD), the sharpness of the crossover depends primarily on the mutual alignment of CDs and for well aligned CDs and field along CDs may result in a kink of $B_{\rm irr}(T)$ for $B_{\rm irr} \sim B_\phi$ [39]. This crossover occurs because the pinning of interstitial vortices for $B_{\rm irr} > B_\phi$ is weaker than for vortices residing on the columns for $B_{\rm irr} < B_\phi$. Therefore, the increase of $B_{\rm irr}(T)$ with decreasing temperature in samples containing CDs becomes slower for $B_{\rm irr}(T) > B_\phi$. Accordingly, if $B_{\rm irr}(T)$ variation for virgin sample (not containing CDs) of the same compound shows no change of slope within the explored temperature interval, the ratio $B_{\rm irr,CD}/B_{\rm irr,virg}$ should achieve maximum value for $B_{\rm irr,CD} \sim B_\phi$. Since $B_{\rm irr}(T)$ increases with decreasing temperature, maximum of the ratio $B_{\rm irr,CD}/B_{\rm irr,virg}$ should shift to lower temperatures on increasing $B_\phi$ (i.e. the density $n_\phi$ of correlated defects providing strong vortex pinning). This

phenomenon is observed in our Ag/Bi2223 tapes containing randomly splayed CDs (Fig. 3b) and somewhat surprisingly it also appears in our $MgB_2$ samples doped with Si-nanoparticles (Fig. 3a). Accordingly, from Figs. 2b and 3b we deduced $B_\phi$ values for U/n processed Bi2223/Ag samples (Table 1) which agree very well with the independent estimates based on topology and density of CDs [32] in our samples. Similarly, from Figs. 2a and 3a we estimate $B_\phi \approx 0.15$, 0.3 and 0.6 T (Table 1) for 5 wt% Si-doped wire, 5 wt% Si-doped tape and 10 wt% Si-doped tape, respectively. Therefore, in our $MgB_2$ samples doped with Si-nanoparticles, $B_\phi$ (and $n_\phi$) seems to increase with increasing Si-content and moreover $B_\phi$ is proportional to Si-content for the samples of the same type (tapes). From the values of $B_\phi$, we estimate $n_\phi \approx 7 \cdot 10^{13}$ to $30 \cdot 10^{13}$ m$^{-2}$ for our doped samples. It is interesting to compare our estimated $n_\phi$s with the results of microstructural studies for nanoparticle doped $MgB_2$.

The microstructural studies of the nanoparticle-doped $MgB_2$ [27, 28, 29] show finely dispersed precipitates within the $MgB_2$ matrix with sizes $\sim$ 10 nm. For Si and SiC doped $MgB_2$ [28, 29], these precipitates are mainly $Mg_2Si$ phase, and their average density compares well with $n_\phi$ values estimated above. Therefore, in our tapes $Mg_2Si$ nanoprecipitates, resulting from the reaction of Si-nanoparticles and Mg during the sintering, act analogously to columnar defects in HTS. This outcome appears rather surprising considering different nature and geometries of precipitates and columns, as well as the different nature of vortices [6, 40] in these materials. The matching effects are common in type-II superconductors [41] and are not specific only to HTS. However, we note two important differences between vortex pinning in nanoparticle doped $MgB_2$ and HTS containing CDs. Firstly, $B_\phi$ (hence $n_\phi$) in doped $MgB_2$ samples depends not only on Si-content, but also on the type of sample (tape or wire). This probably arises from the fact that the preparation technique of $MgB_2$/Cu samples is still not optimized, which shows up in the strong random variation of $J_{c0}$ values (Table 1) for $MgB_2$ samples. (For Bi2223/Ag tapes, $J_{c0}$ values show weak variation, Table 1.) Secondly, the enhancement of $B_{irr}$ for $B_{irr} > B_\phi$ in doped $MgB_2$ samples remains high, and moreover, tends to saturate (Fig. 3a), whereas in HTS samples this enhancement rapidly decreases for $B_{irr} > B_\phi$ (Fig. 3b) and usually vanishes for $B_{irr} \approx 3B_\phi$ [35]. The favourable effect of the enhanced vortex pinning in Si-doped $MgB_2$ samples for $B \gg B_\phi$ may arise from the alloying effects (which show up in a modest decrease of $T_{c0}$ on increasing Si-content, Table 1) and/or from some other defects [28].

Different dominant vortex pinning mechanisms in virgin and nanostructured samples imply also different field variations of their $J_c$ and $F_p = J_c B$. In Fig. 4a, we compare the $J_c(B)$ variations for undoped $MgB_2$ wire and tape doped with 10 wt% Si at the same reduced temperatures $t \geq 0.84$. The undoped sample shows approximately exponential $J_c(B)$ variation, which is typical for $MgB_2$ samples [11, 19, 23, 28]. At low temperatures (high $I_c$), the large self-field $\mu_0 H_s$ makes $J_c(B < \mu_0 H_s)$ nearly constant, whereas at elevated fields ($B \to B_{irr}$), $J_c$ rapidly decreases to zero. The $J_c(B)$ variation of doped $MgB_2$ sample is quite different from that for the undoped tape. The S-shaped $J_c(B)$ curves of doped tape are reminiscent of those observed in HTS films, tapes (Fig. 4b) and crystals containing CDs [6].

Further, for the same reduced temperature $t$, the decrease of $J_c$ with $B$ in the doped tape is much smaller than that for the undoped one. In particular, for $t \approx 0.85$,

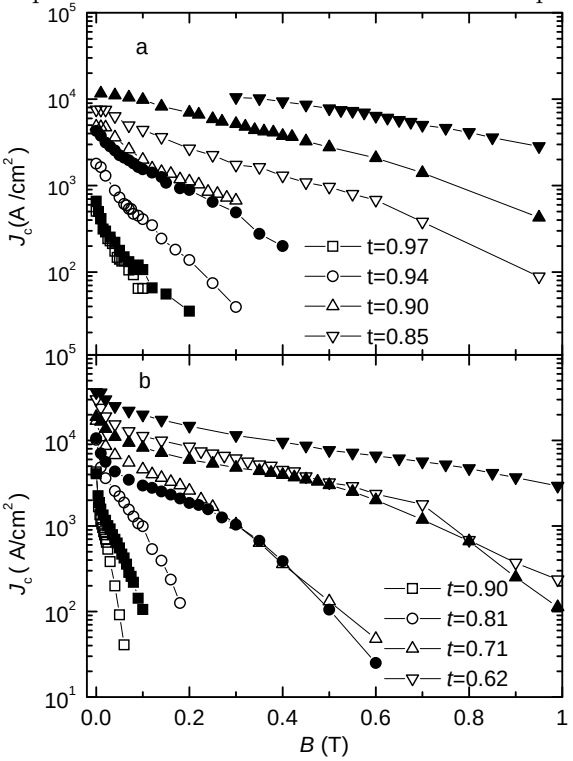


*Fig. 4. Field variation of critical current density $J_c$ at reduced temperatures denoted on plot for the: a) $MgB_2$ undoped wire (empty) and 10 wt% Si-doped tape (full symbols) and b)* Bi2223/Ag *undoped tape (empty) and tape with $B_\phi$ = 0.54 T (full symbols).*

the relative decrease of the critical current density $J_c(0.95\ \mathrm{T})/J_c(0\ \mathrm{T})$ for doped sample is about 16 times smaller than that of the undoped one. Qualitatively, the same behaviour was observed for all doped samples. Accordingly, the nanoparticle doping enhances vortex pinning throughout the vortex-solid regime [6].

As illustrated in Fig. 4b, the effect of CDs on $J_c(B)$ curves of Bi2223/Ag tapes is qualitatively the same as that of nanoprecipitates in $MgB_2$ (Fig. 4a). Since samples in Fig. 4a and 4b have nearly the same $B_\phi$, it is interesting to compare their $J_c(B)$ variation at the same $t$. $J_c(t = 0.9)$ of U/n treated Bi2223/Ag tape vanishes for $B \sim 0.1$ T, whereas $J_c(t = 0.9)$ for Si-doped $MgB_2$ tape remains large even at $B = 0.95$ T. This shows great potential of nanoparticle-doped $MgB_2$. $J_c(B)$ curves for all U/n processed samples showed enhanced vortex pinning and, like in Si-doped $MgB_2$, this enhancement increased and persisted to higher fields on increasing $B_\phi(n_\phi)$.

From the experimental $J_c(B,T)$ results, we obtained the corresponding pinning force density $F_p(B,T)$ curves for all samples. In a case of one dominant vortex pinning mechanism, the shape of $F_p(B)$ curves (especially the ratio $B_{max}/B_{irr}$) may reveal this mechanism [3]. Both for Bi2223/Ag and $MgB_2$/Cu systems, we observed significant difference between $B_{max}/B_{irr}$ for nanostructured and vir-

gin samples. In particular, in U/n processed Bi2223/Ag tapes, we observed [35] $B_{\rm max}/B_{\rm irr} \approx 0.43$ within the temperature region in which vortex pinning on CDs dominates ($B_{\rm irr}$(U/n) > $B_{\rm irr}$(virg). This ratio is consistent with $\Delta T_{\rm c}$-pinning mechanism anticipated for CDs [6] and is quite different from $B_{\rm max}/B_{\rm irr} \leq 0.3$ observed in virgin tapes [9] over the entire temperature range ($t \geq 0.62$). For the undoped $MgB_2$ samples, we found $B_{\rm max}/B_{\rm irr} \approx 0.22$, which is similar to that observed in $Nb_3Sn$ [3] and is consistent with a commonly accepted grain–boundary pinning mechanism for a bulk $MgB_2$ [12].

The enhancement of $B_{\rm max}(t)$ in the doped $MgB_2$ samples is larger than that of $B_{\rm irr}(t)$, which results in $B_{\rm max}(t)/B_{\rm irr}(t) \approx 0.29$ for $t \leq 0.98$. Such $B_{\rm max}/B_{\rm irr}$ ratio is unlikely to arise only from the grain boundary pinning [3] and was earlier observed for U/n treated Bi2223/Ag tapes [9] with a modest density of splayed columnar defects ($B_\phi \lesssim 0.2$ T). Therefore, we propose that $B_{\rm max}/B_{\rm irr} \approx 0.29$ arises from the competition of at least two pinning mechanisms (for example, the grain boundary pinning and the core pinning at nanoprecipitates) as was the case in Bi2223/Ag tapes. A detailed investigation of $J_{\rm c}(B)$ curves extending over a broad temperature range (which requires $I > 200$ A) is necessary in order to solve this problem.

In an attempt to extend our results to lower temperatures, we made an approximate analysis of published $J_{\rm c}(B)$ curves (derived from magnetization measurements) for nanoparticle doped $MgB_2$ samples [27, 28, 29]. The extracted $B_{\rm max}$ values in general increase with the nanoparticle content ($c$) at all explored temperatures ($T \geq 4.2$ K). The corresponding enhancement of $B_{\rm max}$ due to nanoparticles is often linear in $c$, which lends further support to our analysis.

## 4. Conclusions

Taken together, our results for U/n processed Bi2223/Ag tapes and Si-nanoparticle-doped $MgB_2$/Cu samples are consistent with the knowledge gained from the development of practical low-temperature superconductors (NbTi, $Nb_3Sn$): the efficiency of flux pinning depends on our ability to introduce the defects with relevant dimensions $d \sim \xi$ within the superconductor, which strongly and abruptly alter its superconducting properties. Indeed, in both investigated systems, the efficiency of defects (splayed CDs or nanoprecipitates) stems from the fact that $d \sim \xi$ is fulfilled over sizable temperature range. As regards the $B - T$ phase space, the efficiency of flux pinning in these systems persists to higher field ($B_{\rm irr}$) on increasing the density of defects. Further, we observe in both systems quite pronounced matching effects, i.e. the relative enhancement of vortex pinning caused by defects is the largest when the areal density of defects approximately matches that of vortices, $n_\phi$.

In addition to these features, which are common to all type-II superconductors of potential technological interest, the investigated systems also show some novel features not to be found in either conventional nor in high-temperature superconductors. To our knowledge, nanoparticle doped $MgB_2$ is the only superconducting compound which contains nanoprecipitates within its grains. This offers the unique

opportunity to apply the approach for the optimization of flux pinning similar to that used in modern NbTi (an alloy) wires, i.e. to tune simultaneously the grain and precipitate shapes and sizes. Such an approach is likely to produce remarkably efficient vortex pinning over a large portion of $B - T$ phase space. Unfortunately, present-day $MgB_2$/Cu tapes exhibit wild variation in their superconducting properties (see $J_{c0}$ values in Table 1), a problem which has to be solved in order to make practical superconductors.

Similarly, the U/n processed Bi2223/Ag tapes are a unique HTS system containing CDs without the use of high-energy particles. Further, the pinning of vortices by CDs in this system is both isotropic and very strong. The main problems here are the detrimental effects of U-oxide on $J_c$ (which can be partially circumvented by simultaneous optimization of $c$ and $\Phi$ [9]) and the radiation induced in Ag-sheathing.

*Acknowledgements*

We thank Professor S. X. Dou and his group (especially Drs X. L. Wang, D. Milliken, S. Soltanian, M. Delfany) and Dr. R. Weinstein for giving us samples and many usefull suggestions.

References

[1] M. Tinkham, Introduction to Superconductivity, McGraw Hill, Inc., New York (1996).

[2] C. Meingast and D. C. Larbalestier, J. Appl. Phys. **66** (1989) 5971.

[3] D. Dew-Hughes, Philos. Mag. B **55** (1987) 459.

[4] J. G. Bednorz and K. A. Müller, Z. Phys. B **64** (1986) 189.

[5] J. R. Clem, Supercond. Sci. Tech. **11** (1998) 909.

[6] G. Blatter, M. V. Feigel'man, V. B. Geshkenbein, A. I. Larkin and V. M. Vinokur, Rev. Mod. Phys. **66** (1994) 1125.

[7] H. Kumakura, K. Togano, H. Maeda, J. Kase and T. Morimoto, Appl. Phys. Lett. **58** (1991) 2830.

[8] L. Civale, Supercond. Sci. Tech. **10** (1997) A52.

[9] E. Babić et al., Solid State Commun. **118**(2001) 607; G. W. Schulz, C. Klein, H. W. Weber, S. Moss, R. Zeng, S. X. Dou, R. Sawh, Y. Ren and R. Weinstein, Appl. Phys. Lett. **73** (1998) 3935.

[10] J. Nagamatsu, N. Nagakawa, T. Muranaka, Y. Zenitani and J. Akimitsu, Nature **410** (2001) 63.

[11] C. Buzea and T. Yamashita, Supercond. Sci. Tech. **14** (2001) R115.

[12] D. C. Larbalestier et al., Nature **410** (2001) 186.

[13] B. A. Glowacki, M. Majoros, M. Vickers, J. E. Evetts, Y. Shi and I. McDougall, Supercond. Sci. Tech. **14** (2001) 193.

[14] I. Kušević, Ž. Marohnić, E. Babić, Đ. Drobac, X. L. Wang and S. X. Dou, Solid State Commun. **122**(2002) 347.

[15] G. Grasso, A. Malagoli, C. Ferdeghini, S. Roncallo, V. Braccini, A. S. Siri and M. R. Cimberle, Appl. Phys. Lett. **79** (2001) 230.

[16] S. Jin, H. Mavoori, C. Bower and R. B. van Dover, Nature **411** (2001) 563.

[17] S. Soltanian, X. L. Wang, I. Kušević, E. Babić, A. H. Li, H. K. Liu, E. W. Collings and S. X. Dou, Physica C **361** (2001) 84; X. L. Wang, Q. W. Yao, J. Horvat, M. J. Qin and S. X. Dou, Supercond. Sci. Tech. **17** (2004) L21.

[18] H. L. Suo, C. Beneduce, M. Dhallè, N. Musolino, J. Y. Genoud and R. Flükiger, Appl. Phys. Lett. **79** (2001) 3116.

[19] D. K. Finnemore, J. E. Ostenson, S. L. Bud'ko, G. Lapertot and P. C. Canfield, Phys. Rev. Lett. **86** (2001) 2420.

[20] C. B. Eom et al., Nature **411** (2001) 558.

[21] Y. Feng, Y. Zhao, Y. P. Sun, F. C. Liu, B. Q. Fu, L. Zhou, C. H. Cheng, N. Koshizuka and M. Murakami, Appl. Phys. Lett. **79** (2001) 3983.

[22] M. R. Cimberle, M. Novak, P. Manfrinetti and A. Palenzona, Supercond. Sci. Technol. **15** (2002) 43.

[23] Y. Bugoslavsky, L. F. Cohen, G. K. Perkins, M. Polichetti, T. J. Tate, R. G. William and A. D. Caplin, Nature **411** (2001) 561.

[24] E. Babić, Đ. Miljanić, K. Zadro, I. Kušević, Ž. Marohnić, Đ. Drobac, X. L. Wang and S. X. Dou, FIZIKA A **10** (2001) 87.

[25] M. Eisterer, B. A. Glowacki, H. W. Weber, L. R. Greenwood and M. Majoros, Supercond. Sci. Technol. **15** (2002) 1088.

[26] A. Gumbel, J. Eckert, G. Fuchs, K. Nenkov, K. H. Müller and L. Schultz, Appl. Phys. Lett. **80** (2002) 2725.

[27] J. Wang, Y. Bugoslavsky, A. Berenov, L. Cowey, A. D. Caplin, L. F. Cohen, J. L. M. Driscoll, L. D. Cooley, X. Song and D. C. Larbalestier, Appl. Phys. Lett. **81** (2002) 2026.

[28] S. X. Dou, S. Soltanian, J. Horvat, X. L. Wang, S. H. Zhou, M. Ionescu, H. K. Liu, P. Munroe and M. Tomsic, Appl. Phys. Lett. **81** (2002) 3419.

[29] X. L. Wang, S. Soltanian, M. James, W. W. Jao, M. J. Qin, J. Horvat, H. K. Liu and S. X. Dou, Physica C (2003), in press.

[30] I. Kušević, E. Babić, O. Husnjak, S. Soltanian, X. L. Wang and S. X. Dou, (2003) Preprint cond-mat/0311425.

[31] R. Zeng, B. Ye, J. Horvat, Y. C. Guo, B. Zeimetz, X. F. Yang, T. P. Beales, H. K. Liu and S. X. Dou, Physica C **307** (1998) 29.

[32] H. Safar et al., Appl. Phys. Lett. **67** (1995) 130.

[33] M. Majoros, B. A. Glowacki and M. E. Vickers, Supercond. Sci. Technol. **15** (2002) 269.

[34] E. Babić, I. Kušević, S. X. Dou, H. K. Liu and Q. Y. Hu, Phys. Rev. B **49** (1994) 15312.

[35] I. Kušević, E. Babić, D. Marinaro, S. X. Dou and R. Weinstein, Physica C (2003) in press.

[36] D. di Gioacchino, U. Gambardella, P. Tripodi and G. Grimaldi, Supercond. Sci. Technol. **16** (2003) 534.

[37] L. Krusin-Elbaum, L. Civale, G. Blatter, A. D. Marwick, F. Holtzberg and C. Feild, Phys. Rev. Lett. **72** (1994) 1914.

[38] C. J. van der Beek, M. Konczykowski, V. M. Vinokur, T. W. Li, P. H. Kes and G. W. Crabtree, Phys. Rev. Lett. **74** (1995) 1214.

[39] A. Daignère, A. Maignan, V. Hardy and Ch. Simon, Supercond. Sci. Technol. **14** (2001) 659.

[40] M. R. Eskildsen, M. Kugler, S. Tanaka, J. Jun, S. M. Kazakov, J. Karpinski and Ø. Fischer, Phys. Rev. Lett. **89** (2002) 187003.

[41] J. Petermann, Z. Metall. **61** (1970) 724.

## ZAPINJANJE MAGNETSKIH VRTLOGA I KRITIČNE STRUJE U NOVIM NANOSTRUKTURIRANIM SUPRAVODIČIMA

Predstavljamo sustavnu analizu parametara zapinjanja magnetskih vrtloga u novim supravodičima koji sadrže jake izotropne nanoskopske centre zapinjanja kao što su Bi2223/Ag trake obrađene sa U/n i $MgB_2$ punjen nanočesticama silicija. Iako su ti materijali vrlo različiti u pogledu kristalne strukture, prirode vrtloga i nanoskopskih defekata, njihovi parametri zapinjanja vrtloga (ireverzibilna polja i polja maksimalne volumne sile zapinjanja) pokazuju izrazito slična svojstva. Npr., u tim je materijalima pojačanje zapinjanja vrtloga pri umjerenim gustoćama defekata $n_\phi$ približno linearno s $n_\phi$ u širokom području temperatura i magnetskih polja. Ukratko, ti materijali pokazuju učinke usklađivanja s efektivnim poljima usklađivanja $B_\phi$ razmjernim $n_\phi$. Polje $B_\phi$ čini prirodnu ljestvicu polja za zapinjanje vrtloga u takvim sustavima. Međutim, u poljima daleko od $B_\phi$ dolazi do miješanja različitih mehanizama zapinjanja vrtloga. Sažeto se razmatra utjecaj ovih saznanja na buduće pojačanje zapinjanja vrtloga u nanostrukturiranim Bi2223 i $MgB_2$ supravodičima.